Monthly Notices
of the
ROYAL ASTRONOMICAL SOCIETY

MNRASL **436,** L35–L39 (2013)
Advance Access publication 2013 August 30

doi:10.1093/mnrasl/slt107

Detection of water absorption in the day side atmosphere of HD 189733 b using ground-based high-resolution spectroscopy at 3.2 μm⋆

J. L. Birkby,[1]† R. J. de Kok,[2] M. Brogi,[1] E. J. W. de Mooij,[3] H. Schwarz,[1] S. Albrecht[4] and I. A. G. Snellen[1]

[1]*Leiden Observatory, Leiden University, Niels Bohrweg 2, 2333 CA Leiden, the Netherlands*
[2]*SRON Netherlands Institute for Space Research, Sorbonnelaan 2, 3584 CA Utrecht, the Netherlands*
[3]*Department of Astronomy and Astrophysics, University of Toronto, 50 St. George Street, Toronto, ON M5S 3H4m, Canada*
[4]*Department of Physics, and Kavli Institute for Astrophysics and Space Research, Massachusetts Institute of Technology, Cambridge, MA 02139, USA*

Accepted 2013 August 1. Received 2013 July 23; in original form 2013 July 4

ABSTRACT

We report a 4.8σ detection of water absorption features in the day side spectrum of the hot Jupiter HD 189733 b. We used high-resolution ($R \sim 100\,000$) spectra taken at 3.2 μm with CRIRES on the VLT to trace the radial-velocity shift of the water features in the planet's day side atmosphere during 5 h of its 2.2 d orbit as it approached secondary eclipse. Despite considerable telluric contamination in this wavelength regime, we detect the signal within our uncertainties at the expected combination of systemic velocity ($V_{\rm sys} = -3^{+5}_{-6}$ km s^{-1}) and planet orbital velocity ($K_{\rm p} = 154^{+14}_{-10}$ km s^{-1}), and determine a H_2O line contrast ratio of $(1.3 \pm 0.2) \times 10^{-3}$ with respect to the stellar continuum. We find no evidence of significant absorption or emission from other carbon-bearing molecules, such as methane, although we do note a marginal increase in the significance of our detection to 5.1σ with the inclusion of carbon dioxide in our template spectrum. This result demonstrates that ground-based, high-resolution spectroscopy is suited to finding not just simple molecules like CO, but also to more complex molecules like H_2O even in highly telluric contaminated regions of the Earth's transmission spectrum. It is a powerful tool that can be used for conducting an immediate census of the carbon- and oxygen-bearing molecules in the atmospheres of giant planets, and will potentially allow the formation and migration history of these planets to be constrained by the measurement of their atmospheric C/O ratios.

Key words: techniques: spectroscopic – stars: individual: HD 189733 – planetary systems.

1 INTRODUCTION

In the past three years, high-resolution, near-infrared, ground-based spectroscopy has identified the signature of molecular absorption by carbon monoxide (CO) in the atmospheres of several hot Jupiters, including in the transmission spectrum of HD 209458 b (Snellen et al. 2010), and in the thermal day side spectra of the transiting planet HD 189733 b (de Kok et al. 2013; Rodler et al. 2013), and the non-transiting planets τ Boötis b (Brogi et al. 2012; Rodler et al. 2012) and tentatively 51 Pegasi b (Brogi et al. 2013). The more significant of these detections have been made with the CRyogenic high-resolution InfraRed Echelle Spectrograph (CRIRES; Kaeufl et al. 2004) on the Very Large Telescope (VLT) at a resolution of $R \sim 100\,000$ targeting the individual lines of the CO band head at 2.3 μm. The large change in the radial velocity of the planets ($\sim$100 km s^{-1}) during their orbits allows their spectra to be disentangled from the essentially stationary lines of their host stars and from the Earth's static telluric lines. A simple cross-correlation of the extracted planet spectrum with models of CO transitions for different atmospheric temperature–pressure (T/P) profiles and volume mixing ratios (VMRs) not only revealed the presence of CO in the planetary atmosphere, but also allowed the planet's orbital velocity and hence its orbital inclination to be calculated. In the cases of the transiting planets, this allowed them to be treated as eclipsing binary systems, resulting in model-independent measurements of the true masses and radii of the host star and planet. Ground-based, high-resolution spectroscopy is clearly a powerful technique for characterizing exoplanets and their atmospheres (Snellen et al. 2013), but its potential for detecting other molecules, in particular the other main carbon- and oxygen-bearing species, such as water (H_2O), methane (CH_4) and carbon dioxide (CO_2), is as yet untested, particularly in more opaque regions of the Earth's atmosphere. Ultimately, the technique can be used to provide constraints on the relative abundances of these molecules in planetary atmospheres, and hence an estimate of the carbon-to-oxygen ratio (C/O), which is

⋆Based on observations collected at the European Southern Observatory (186.C-0289).

† E-mail: birkby@strw.leidenuniv.nl

thought to have strong implications for the formation and migration history of the planets (see e.g. Lodders 2004; Öberg et al. 2011).

HD 189733 b is one of the most studied exoplanets to date, with strong evidence for a high-altitude haze that causes Rayleigh scattering from 0.3 to 1 μm (Pont et al. 2008; Sing et al. 2009, 2011; Pont et al. 2013), reports of H_2O absorption features at infrared wavelengths (Tinetti et al. 2007; Grillmair et al. 2008; Swain et al. 2008) and claims of CH_4 fluorescence at 3.25 μm (Swain et al. 2010; Waldmann et al. 2012). However, there is some interesting debate in the literature about the latter two spectral features with both systematics and the possible haze being proposed as the causes of conflicting results at different wavelengths (Ehrenreich et al. 2007; Grillmair et al. 2007; Désert et al. 2009; Sing et al. 2009; Gibson et al. 2011; Mandell et al. 2011; Gibson et al. 2012). In this Letter, we present $R \sim 100\,000$ time-resolved CRIRES spectra of the hot Jupiter HD 189733 b, centred on 3.2 μm, targeted at detecting the potential molecular signatures of CH_4, H_2O and also CO_2 in the planetary atmosphere. Our choice to observe at 3.2 μm was driven by the claimed detection of methane fluorescence in this region for HD 189733 b, which would produce easily identifiable emission features in the residuals of our high-resolution spectra given the ∼1 per cent emission features seen at much lower resolution by Swain et al. (2010). However, the 3.2 μm region probed by CRIRES suffers almost total telluric absorption in some parts (unlike previous observations at 2.3 μm) which has the potential to degrade the results of the cross-correlation technique as there will be fewer pixels to use in the analysis. In addition, the molecular spectra of H_2O, CH_4 and CO_2 are far more complex than the CO spectra used in our previous analysis, with many lines that are extremely weak at the temperatures accessible to laboratory measurements. Accurate line positioning in the models is key to the success of the cross-correlation technique, but ab initio calculations are necessary to generate the hot model spectra we require. This may result in small errors in the line positions (Bailey & Kedziora-Chudczer 2012), but water vapour lines are well constrained by observations (Barber et al. 2006).

2 OBSERVATIONS AND DATA REDUCTION

2.1 Observations

We observed HD 189733 (K1V, $V = 7.68$ mag, $K = 5.54$ mag) as part of the large ESO programme 186.C-0289, which was designed to detect the spectral signatures of molecular species in the atmospheres of the brightest known transiting and non-transiting systems accessible from Chile. We observed the target for ∼5 h during the night of 2011 August 1, using CRIRES mounted at Nasmyth A focus on the 8.2-m telescope UT1 (Antu) of the VLT, located on Cerro Paranal in Chile. The observations were carried out in combination with the Multi-Application Curvature Adaptive Optic system (MACAO; Arsenault et al. 2003) and a 0.2 arcsec slit centred on 3236 nm (order 17). CRIRES consists of four Aladdin III InSb-arrays each spanning 1024 × 512 pixel, with a gap of ∼280 pixel between each chip. The resulting wavelength coverage of our observations was thus $3.1805 < \lambda(\mu\text{m}) < 3.2659$ with a resolution of $R \sim 100\,000$ per resolution element. The planet was observed without interruption between orbital phases of $0.383 < \phi < 0.475$ as the maximum day side illumination of the planet was rotating into view, corresponding to a total planet radial-velocity change of $\sim 75\,\text{km s}^{-1}$. In total, we obtained 48 spectra, with each spectrum consisting of two sets of 5 × 30 second exposures. To allow for accurate sky-background subtraction, the telescope was nodded along the slit by 10 arcsec between each set of exposures in an ABBA sequence. A standard set of calibration frames was taken the following morning.

2.2 Basic data reduction

We carried out the initial two-dimensional (2D) image processing and extraction of the 1D spectra using version 2.2.1 of the CRIRES ESOREX pipeline. The data were flat-fielded and corrected for bad pixels and non-linearity effects, then background-subtracted by combining each AB nodding pair, before using an optimal extraction technique (Horne 1986) to obtain the 1D spectra. The pipeline products require post-processing in order to remove the contaminating telluric features. For this purpose, we used a combination of IRAF routines and custom-built IDL procedures. Each CRIRES detector is read out using a different amplifier, and each has its own particular characteristics that need to be dealt with independently. Consequently, we handled the 1D spectra from each detector separately, creating four matrices of size $1024 \times N$, where N is the number of spectra, sorted in order of time (i.e. phase) along the y-axis, while the x-axis corresponds to pixel number (i.e. wavelength). An example of the matrix created for detector 1 can be seen in the top panel of Fig. 1.

Our first post-processing step was to mask any groups of bad columns in the matrices, i.e. those typically associated with detector defects at the beginning and end of each detector. We then performed an additional bad-pixel correction to fix bad regions and pixels not identified by the pipeline. Singular bad pixels and isolated bad columns were identified by eye. The bad pixels were replaced with spline-interpolated values from their horizontal neighbouring pixels. Additional residual bad pixels were identified iteratively during this process, with a total of 0.2–0.9 per cent of the pixels in each matrix requiring correction. Next, we selected the spectrum in each matrix with the highest signal-to-noise ratio (S/N) as a reference and used it to align all of the spectra on to a common wavelength grid in pixel space. To do this, we made use of the stationary telluric features in the spectra and performed a cross-correlation between each spectrum and the reference using the IRAF task FXCOR. The measured pixel offsets from the reference were applied to each spectrum using a global spline interpolation to align them with the reference spectrum.

We derived a common wavelength solution by identifying the wavelengths of the telluric features in the reference spectrum based on comparison with a synthetic telluric transmission spectrum from ATRAN[1] (Lord 1992). The precipitable water vapour (PWV) content that best represented the atmospheric conditions during our observations was PWV = 2.0 mm. The synthetic spectrum was used to create a line list to pass to the IRAF function IDENTIFY, which we made by selecting the minimum data point in each telluric absorption line of the synthetic spectrum. The IDENTIFY procedure was then used to mark the pixel positions of the selected telluric features in the reference spectrum and a wavelength solution in pixel space was derived using a third-order Chebyshev polynomial. This was used to update the default pipeline wavelength solution.

2.3 Removal of telluric contamination with SYSREM

The 3.2 μm region contains many water absorption lines (see Fig. 2), and the expected depth of these lines in the atmosphere of

[1] http://atran.sofia.usra.edu/cgi-bin/atran/atran.cgi

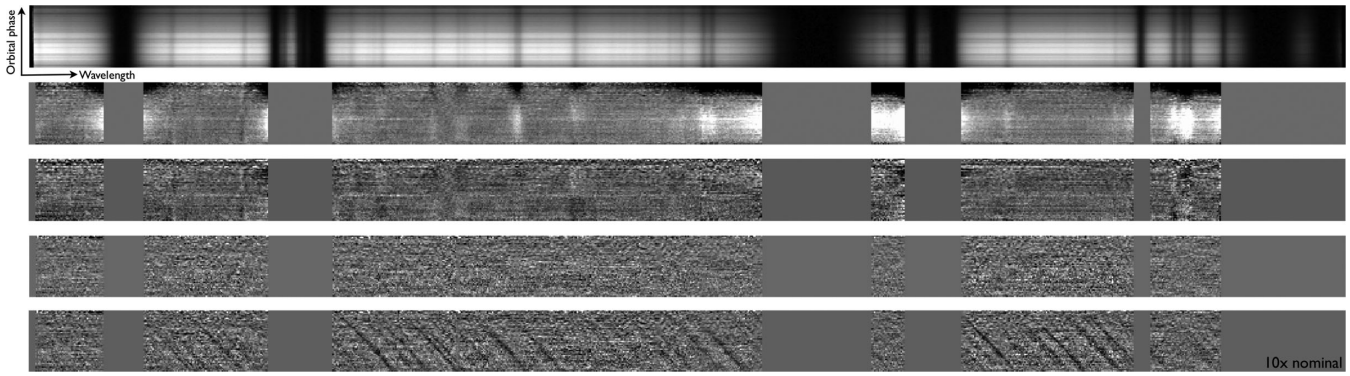

Figure 1. Removal of telluric features on detector 1 by SYSREM iterations. The top panel shows the CRIRES pipeline spectra after aligning to a common wavelength grid. Time (or frame number) increases vertically on the *y*-axis of the matrices, while pixel number increases along the *x*-axis. The second panel shows the residuals of the mean-subtracted spectra given as the first input to SYSREM. The greyed-out regions show where we applied the mask for near total telluric absorption. The third panel shows the residuals after the first iteration of SYSREM which has removed a trend that correlates strongly with air mass. The fourth panel shows the residuals after the optimal number of SYSREM iterations for detector 1 (8 in this case) and after division of each pixel by the squared standard deviation of its column. The standard deviation of this matrix is 4.5×10^{-3}. For reference, the bottom panel shows the same as the fourth panel but with the best-matching cross-correlation template injected at 10 times the nominal value before running SYSREM, to highlight how the planetary lines shift during the night compared to the telluric features.

HD 189733 b, with respect to the stellar continuum, is $\sim 10^{-3}$ (Deming et al. 2006; Charbonneau et al. 2008; Grillmair et al. 2008). Our observed spectra have a typical S/N of ∼200 in the continuum, so the individual water lines of the planet spectrum are buried in the noise of the data. In order to extract the planet signal, we used a cross-correlation technique to combine the contributions from the individual lines (Brogi et al. 2013; de Kok et al. 2013). However, before we can do this, we must first remove the dominant signal of telluric contamination (see Fig. 1). The telluric features remain stationary over the course of the observations and appear as vertical lines in the matrices. However, they change in strength throughout the night due to the varying geometric air mass and fluctuations in the water vapour content of the atmosphere above Paranal. The spectral fingerprint of the planetary atmosphere on the other hand will be Doppler shifted by 10 s of km s^{-1} during the night and will trace out diagonal absorption features across the matrices (see the bottom panel of Fig. 1). In this work, we take a slightly different approach to removing the telluric contamination than in our previous studies as part of our ongoing study to optimise the data reduction. Here, we build upon the method of singular value decompositions (SVDs) used by de Kok et al. (2013) to identify carbon monoxide absorption in high-resolution spectra of the day side of HD 189733 b at 2.3 μm. We have employed the SYSREM algorithm (Tamuz et al. 2005; Mazeh et al. 2007), which is commonly used by transit surveys to de-trend light curves. SYSREM, like SVDs, is able to remove systematic trends without any prior knowledge of the underlying cause, but has been demonstrated to be more effective in cases where the errors per data point are not equal (Tamuz et al. 2005). This is particularly relevant for our 3.2 μm data set due to the broad and deep telluric absorption lines. In our case, we treat each column (or wavelength channel) of the spectral matrix as a 'light curve' consisting of 48 frames. The individual uncertainties on each data point in the matrix are the error calculated by the optimal extraction routine of the CRIRES data reduction pipeline for each pixel in each spectrum. Before executing SYSREM on a per detector basis, we first normalized the spectra to their peak continuum value per detector and masked regions of almost total telluric absorption. Finally, we divided each individual spectrum by its mean pixel value and subtracted unity. An example of the input matrix to SYSREM is shown in Fig. 1. The first systematic component removed by SYSREM tightly correlates with air mass for all four detectors, but subsequent trends do not obviously match with other physical parameters such as seeing or pressure. In order to determine the optimal number of SYSREM iterations to execute, we test which combination of iterations and detectors give the highest significance at the expected planet position. In total, we ran 20 iterations of SYSREM per detector. We found that detectors 2 and 4 did not increase the detection significance for any number of the tested iterations. This is perhaps not surprising for detector 2 given the heavy masking we applied to the near total telluric absorption features (see the top panel of Fig. 2), which left little signal to work with. Detector 4 is known to suffer reduced quality due to known variations in the gain between neighbouring columns (the odd–even effect) caused by the alignment position of the detector, and such issues have prevented the use of detector 4 in some of our previous observations (Brogi et al. 2013). The effect is a zig-zag pattern in the 1D spectra on detector 4 which is static in time with an average amplitude of ±5 per cent around the continuum, but which scales strongly with increasing count level, peaking

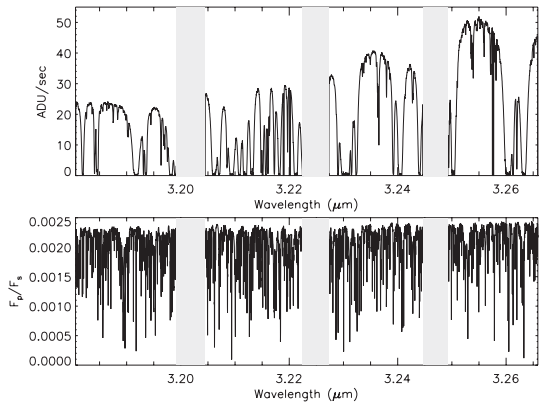

Figure 2. Top: an example of a 1D reduced spectrum from the CRIRES pipeline before removal of the telluric features. The shaded regions mark the gaps between the detectors. Detector 2 suffers significant contamination from water in the Earth's atmosphere. Bottom: the template spectrum of water and carbon dioxide that gave the best cross-correlation value. It is noticeably more complex than the model spectrum used to detect CO (see fig. 7 of de Kok et al. 2013).

at ∼10 per cent in some frames. The optimum combination was to use only detectors 1 and 3, with 8 SYSREM iterations on detector 1 and just one iteration on detector 3. The greater number of iterations required for detector 1 compared to detector 3 may again be due to the odd–even effect as it has the same alignment as detector 4. However, the lower count level on detector 1 compared to detector 4 reduces the effect to almost negligible levels. As a final step before cross-correlation, we divide each pixel by the squared standard deviation of its column.

3 CROSS-CORRELATION ANALYSIS AND RESULTS

The residuals of each spectrum after running SYSREM were cross-correlated with a grid of models convolved to the CRIRES spectral resolution containing molecular signatures of different combinations of CH_4, H_2O and CO_2. The models were generated for the 3.2 μm region in the same way as those used to study the 2.3 μm region in de Kok et al. (2013). At high pressures (≥0.1 bar), the atmospheric temperature was set to 1350 K and it then followed the profiles of Madhusudhan & Seager (2009). For a lower pressure (p_1), the temperature (t_1) was varied from 500 to 1500 K in steps of 500 K, which allowed for a weak thermal inversion at high altitudes. Between 0.1 and p_1 bar we assumed a constant rate of change of temperature with log (pressure), and varied p_1 between $10^{-1.5}$ and 10^{-4} in steps of $10^{0.5}$. The VMRs of the gases were allowed to vary between 10^{-6} and 10^{-3} also in steps of $10^{0.5}$. The cross-correlation analysis was performed over a range of lag values corresponding to planet radial velocities of $-100 \leq \mathrm{RV_p} \leq +200\,\mathrm{km\,s^{-1}}$. As in our previous studies with CRIRES, the maximum cross-correlation signal is found by shifting the cross-correlation functions for each spectrum to the rest frame of the planet and summing over time for a range of planet radial-velocity semi-amplitudes ($20 \leq K_\mathrm{p} \leq 180\,\mathrm{km\,s^{-1}}$). Based on literature values of the planet and host star masses (e.g. Triaud et al. 2009) and the known inclination of the transiting system, the expected planet radial velocity is $K_\mathrm{p} \sim 152\,\mathrm{km\,s^{-1}}$ at $V_\mathrm{sys} = -2.361\,\mathrm{km\,s^{-1}}$ (Bouchy et al. 2005). The best-matching cross-correlation template contained both H_2O and CO_2 absorption lines, with $t_1 = 500$ K, $p_1 = 10^{-1.5}$, $\mathrm{VMR_{H_2O}} = 10^{-5}$ and $\mathrm{VMR_{CO_2}} = 10^{-4}$. However, the detection significance across the full range of temperatures, pressures and VMRs tested for the $H_2O + CO_2$ templates was always within 1σ of the best-matching model, which is shown (before convolution to the CRIRES spectral resolution) in the bottom panel of Fig. 2. The strength of the cross-correlation signal decreased with the inclusion of CH_4 in all cases. A matrix containing the total combined cross-correlation values for the best $H_2O + CO_2$ model is shown in Fig. 3 as a function of V_sys and K_p. The peak value of the cross-correlation matrix is located at $V_\mathrm{sys} = -3^{+5}_{-6}\,\mathrm{km\,s^{-1}}$ and $K_\mathrm{p} = 154^{+14}_{-10}\,\mathrm{km\,s^{-1}}$, which is consistent with literature values for the expected planet position (Bouchy et al. 2005; de Kok et al. 2013). We determine the significance of the detection by dividing the peak value of the cross-correlation matrix by the standard deviation of the whole matrix, which results in a detection significance of 5.1σ for the combined signal of detectors 1 and 3 (individually the two detectors give 4.5σ and 3.0σ, respectively). This approach assumes that the distribution of the cross-correlation values is Gaussian, which is reasonable, despite possible systematics in the observed spectra, because we have (i) normalized each pixel by its uncertainty and (ii) by cross-correlating with a template of many lines that span the entire wavelength range, systematic variations from a Gaussian distribution are heavily down-weighted. However, to test the assumption of Gaussianity, we show the distributions of the cross-correlation values inside and outside the planet radial-velocity trail in Fig. 4. The out-of-trail cross-correlation values are well fitted by the Gaussian curve shown in the plot, and the in-trail values are notably offset from the out-of-trail distribution. A Welch T-test rules out the in-trail and out-of-trail values having been drawn from the same parent distribution at the 4.9σ level.

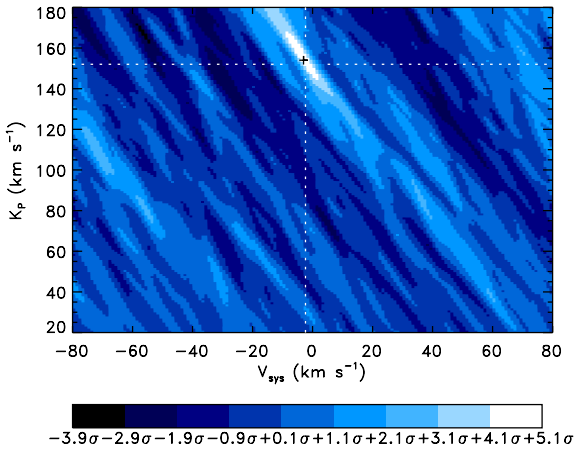

Figure 3. Total cross-correlation values from detectors 1 and 3 after summing over time for a range of systemic velocities (V_sys) and planet radial-velocity semi-amplitude (K_p). The dashed white line marks the expected planet signal based on literature values ($V_\mathrm{sys} = -2.361\,\mathrm{km\,s^{-1}}$, $K_\mathrm{p} = 152\,\mathrm{km\,s^{-1}}$), while the black plus sign marks the position of the maximum cross-correlation value ($V_\mathrm{sys} = -3^{+5}_{-6}\,\mathrm{km\,s^{-1}}$, $K_\mathrm{p} = 154^{+14}_{-10}\,\mathrm{km\,s^{-1}}$), which is consistent with the literature values within our uncertainties. The white contour marks the 1σ region around the peak cross-correlation value.

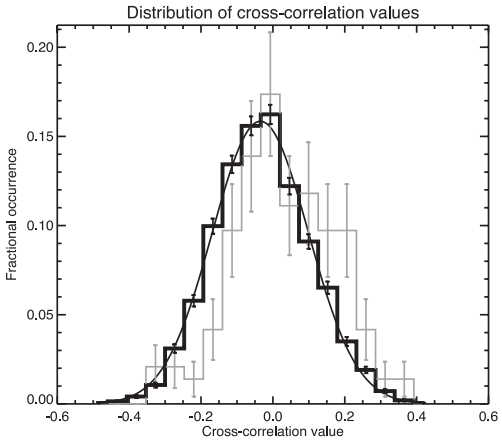

Figure 4. A comparison of the in-trail (grey histogram) and out-of-trail (black histogram) cross-correlation values. The error bars are the square root of the bin occurrences. The out-of-trail values are well fitted by a Gaussian (black curve) and the in-trail values are offset towards higher cross-correlation values. A Welch T-test rejects the hypothesis that the two distributions are drawn from the same parent population at the 4.9σ level.

4 DISCUSSION

The inclusion of CO_2 in the cross-correlation template improves our detection significance, but only marginally (an increase of $\sim 0.3\sigma$); hence, our subsequent discussion is based on the cross-correlation with the best-matching H_2O template only, which gives a detection significance of 4.8σ at the same V_sys and K_p value found with the overall best-matching template. We note here that the data were also

analysed with the SVD method described by de Kok et al. (2013) and the results were the same with similar errors, suggesting that the SVD method still works well even in more telluric-contaminated spectra than at 2.3 μm. In order to determine the line contrast ratio of the H_2O lines (i.e. the depth of the deepest H_2O lines with respect to the continuum divided by the stellar flux), we followed the method of Brogi et al. (2013), injecting an inverse scaled version of the best-matching H_2O model such that the signal at the detected planet position was exactly cancelled. This resulted in a H_2O line contrast ratio of $(1.3 \pm 0.2) \times 10^{-3}$ for the non-convolved model. This is greater than the CO line contrast ratio at 2.3 μm ($[4.5 \pm 0.9] \times 10^{-4}$; de Kok et al. 2013) and we found that in some cases a steep T/P profile was required to match the H_2O result. This could indicate a possible overabundance of H_2O compared to CO, or possibly that the high-opacity haze detected at optical wavelengths continues to partially obscure the CO line depths in the K band. However, within our errors we also find a range of T/P profiles where the two molecules fit to the same T/P profile, meaning that with only these two CRIRES detections, we cannot constrain the gas abundances independently from the T/P profiles. In order to constrain the T/P and abundances further, a full retrieval including both secondary eclipse and transit measurements is required, but is beyond the scope of this Letter. Future high-resolution observations at a wavelength where the signals of several molecules are strong enough to be detected simultaneously will allow much tighter constraints on the relative abundance ratios, because the gases will be reliant on the same T/P profile and continuum level, and will likely probe overlapping regions of pressure (de Kok et al. 2013). Importantly, such measurements would also remove any degeneracy with time-dependent factors, such as weather (Brogi et al. 2013).

Our analysis found no increase in the cross-correlation strength when including methane in the model spectrum, in both absorption and emission for local thermodynamic equilibrium (LTE) chemistry. Here, we assess claims of non-LTE methane emission at the $F_p/F_s \sim 0.9$ per cent level in the atmosphere of HD 189733 b arising from observations with SpeX on NASA's IRTF at ∼3.25 μm with an effective resolving power of $R \sim 30$ (Swain et al. 2010). Such signals can be caused by fluorescence (radiative pumping by incident photons) or other disequilibrium processes. Support for the result was recently published by the same group using new observations with the same instrument at both 3.3 and 2.3 μm, and similarly strong emission was reported in both regions at an effective resolution of $R \sim 175$ (Waldmann et al. 2012). However, Mandell et al. (2011), who observed the system with NIRSPEC on Keck II at a resolving power of $R \sim 27\,000$ ruled out emission features in the L band with upper limits 40 times smaller than expected based on the SpeX results. In a similar approach to Mandell et al. (2011), we note that non-LTE emission lines will not be significantly broadened by collisions in the exoplanet atmosphere, and thus the emission intensity must be brighter at higher spectral resolving power. At the resolving power of CRIRES ($R \sim 100\,000$), we would expect to see line emission $\gg$1 per cent. To test this, we first shifted the residuals of our spectra after running SYSREM to the rest frame of the planet based on our detected K_p, then summed them over time (weighting each column by the number of pixels that had not been masked in that column) to create a stacked 1D spectrum. The largest positive deviation on detectors 1 and 3 in the stacked spectrum (for columns where more than half of the pixels were not masked) was <0.6 per cent, and the standard deviation across both chips was $\lesssim$0.1 per cent. Hence, in agreement with Mandell et al. (2011), our high-resolution spectra do not validate the claims of non-LTE emission at 3.25 μm.

ACKNOWLEDGEMENTS

We would like to thank the VLT/CRIRES night astronomers and telescope operators for their help in conducting our programme, Elena Valenti at ESO User Support for her timely and helpful response, and our anonymous referee for their insightful comments.

REFERENCES

Arsenault R. et al., 2003, Proc. SPIE, 4839, 174
Bailey J., Kedziora-Chudczer L., 2012, MNRAS, 419, 1913
Barber R. J., Tennyson J., Harris G. J., Tolchenov R. N., 2006, MNRAS, 368, 1087
Bouchy F. et al., 2005, A&A, 444, L15
Brogi M., Snellen I. A. G., de Kok R. J., Albrecht S., Birkby J., de Mooij E. J. W., 2012, Nat, 486, 502
Brogi M., Snellen I. A. G., de Kok R. J., Albrecht S., Birkby J. L., de Mooij E. J. W., 2013, ApJ, 767, 27
Charbonneau D., Knutson H. A., Barman T., Allen L. E., Mayor M., Megeath S. T., Queloz D., Udry S., 2008, ApJ, 686, 1341
de Kok R. J., Brogi M., Snellen I. A. G., Birkby J., Albrecht S., de Mooij E. J. W., 2013, A&A, 554, A82
Deming D., Harrington J., Seager S., Richardson L. J., 2006, ApJ, 644, 560
Désert J.-M., Lecavelier des Etangs A., Hébrard G., Sing D. K., Ehrenreich D., Ferlet R., Vidal-Madjar A., 2009, ApJ, 699, 478
Ehrenreich D., Hébrard G., Lecavelier des Etangs A., Sing D. K., Désert J.-M., Bouchy F., Ferlet R., Vidal-Madjar A., 2007, ApJ, 668, L179
Gibson N. P., Aigrain S., Pont F., Sing D. K., Désert J.-M., Evans T. M., Henry G., Husnoo N., Knutson H., 2012, MNRAS, 422, 753
Gibson N. P., Pont F., Aigrain S., 2011, MNRAS, 411, 2199
Grillmair C. J., Charbonneau D., Burrows A., Armus L., Stauffer J., Meadows V., Van Cleve J., Levine D, 2007, ApJ, 658, L115
Grillmair C. J. et al., 2008, Nat, 456, 767
Horne K., 1986, PASP, 98, 609
Kaeufl H.-U. et al., 2004, Proc. SPIE, 5492, 1218
Lodders K., 2004, ApJ, 611, 587
Lord S. D., 1992, in NASA Technical Memorandum 103957
Madhusudhan N., Seager S., 2009, ApJ, 707, 24
Mandell A. M., Drake Deming L., Blake G. A., Knutson H. A., Mumma M. J., Villanueva G. L., Salyk C., 2011, ApJ, 728, 18
Mazeh T., Tamuz O., Zucker S., 2007, in Afonso C., Weldrake D., Henning Th., eds, ASP Conf. Ser. Vol. 366, Transiting Extrasolar Planets Workshop. Astron. Soc. Pac., San Francisco, p. 119
Öberg K. I. et al., 2011, ApJ, 743, L16
Pont F., Knutson H., Gilliland R. L., Moutou C., Charbonneau D., 2008, MNRAS, 385, 109
Pont F., Sing D. K., Gibson N. P., Aigrain S., Henry G., Husnoo N., 2013, MNRAS, 432, 2917
Rodler F., Kürster M., Barnes J. R., 2013, MNRAS, 432, 1980
Rodler F., Lopez-Morales M., Ribas I., 2012, ApJ, 753, L25
Sing D. K., Désert J.-M., Lecavelier Des Etangs A., Ballester G. E., Vidal-Madjar A., Parmentier V., Hebrard G., Henry G. W., 2009, A&A, 505, 891
Sing D. K. et al., 2011, MNRAS, 416, 1443
Snellen I. A. G., de Kok R. J., de Mooij E. J. W., Albrecht S., 2010, Nat, 465, 1049
Snellen I. A. G., de Kok R. J., le Poole R., Brogi M., Birkby J., 2013, ApJ, 764, 182
Swain M. R., Vasisht G., Tinetti G., 2008, Nat, 452, 329
Swain M. R. et al., 2010, Nat, 463, 637
Tamuz O., Mazeh T., Zucker S., 2005, MNRAS, 356, 1466
Tinetti G. et al., 2007, Nat, 448, 169
Triaud A. H. M. J. et al., 2009, A&A, 506, 377
Waldmann I. P., Tinetti G., Drossart P., Swain M. R., Deroo P., Griffith C. A., 2012, ApJ, 744, 35

This paper has been typeset from a TEX/LATEX file prepared by the author.